

# Forcing of the MJO-related Indian Ocean Heating on the Intraseasonal Lagged NAO

**Xiaolu Shao<sup>1</sup>, David M. Straus<sup>2</sup>, Shuanglin Li<sup>3,5</sup>, Erik T. Swenson<sup>2</sup>, Priyanka Yadav<sup>2</sup>, and  
Jie Song<sup>4</sup>**

<sup>1</sup>College of Oceanography, Hohai University, Nanjing, China, <sup>2</sup>Department of Atmospheric,  
Oceanic and Earth Sciences, George Mason University, Fairfax, Virginia, United States,  
<sup>3</sup>Climate Change Research Center, Institute of Atmospheric Physics, Chinese Academy of  
Sciences, Beijing, China, <sup>4</sup>LASG, Institute of Atmospheric Physics, Chinese Academy of  
Sciences, Beijing, China, <sup>5</sup>Department of Atmospheric Science, China University of  
Geosciences, Wuhan, China

Corresponding author: Shuanglin Li ([shuanglin.li@mail.iap.ac.cn](mailto:shuanglin.li@mail.iap.ac.cn))

## **Key Points:**

- The lagged connection of the NAO with the MJO is reproduced well in the CFSv2 model with prescribed cyclic MJO heating forcings
- The MJO-related heating (cooling) over the Indian Ocean alone plays a dominant role in the formation of the positive (negative) NAO anomaly
- The MJO affects the NAO via a secondary Eurasian (westward oriented) pathway, and the primary North Pacific (eastward oriented) pathway

## **Abstract**

Based on the experiments with the Coupled Forecast System version 2 (CFSv2), the mechanism by which the Madden–Julian Oscillation (MJO) modulates the North Atlantic Oscillation (NAO) is investigated. To isolate the cyclic MJO heating with an eastward propagation over the Indian Ocean and western Pacific, three sets of experiments are conducted with spatio-temporal varying heating added to the model’s internally generated heating. The results suggest that the anomalous MJO heating over the Indian Ocean, rather than the western Pacific, dominates the formation of the NAO anomaly in the following 10–20 days. The MJO heating triggers a westward propagation of the storm track that influences Europe, complementing the eastward pathway of influence via the North Pacific. Both pathways contribute to an enhanced storm track over the North Atlantic and the positive NAO anomaly. The Eurasian pathway is less important for the formation of the negative NAO anomaly.

## **Plain Language Summary**

As the dominant source of predictability for subseasonal forecasts, the Madden–Julian Oscillation (MJO) has a great impact on the leading winter extratropical mode, the North Atlantic Oscillation (NAO). Previous studies suggested that the impact is through the downstream propagation of the MJO-excited Rossby wave across the North Pacific and its interaction with synoptic eddies over the North Atlantic. In addition to the traditional Pacific pathway, here we find another pathway by which the MJO convection over the Indian Ocean triggers a westward propagation of the Asian storm track that penetrates Eurasia and influence the wave–eddy interaction related to the NAO.

## **1 Introduction**

The North Atlantic Oscillation (NAO), one of the dominant mode of the extratropical atmospheric variability, has a significant influence on weather and climate over the wide northern hemisphere (Hurrell et al., 2003). The NAO varies temporally with periods spanning a broad spectrum from synoptic to decadal, and its activity at intraseasonal timescale is one substantial source of extended-range weather forcecasting. To predict NAO activity at intraseasonal timescales is thus of substantial importance.

The Madden–Julian Oscillation (MJO), the prominent mode of tropical intraseasonal variability, is characterized with large-scale convection propagating eastward through the Indian Ocean and the western Pacific along with baroclinic atmospheric circulation anomalies (Madden & Julian, 1994; Zhang, 2005). Since the associated heating drives atmospheric teleconnections, the MJO has a great impact on the extratropical atmospheric circulations (Garfinkel et al., 2014; Matthews et al., 2004; Seo & Son, 2012; Stan et al., 2017; Zheng & Chang, 2019).

Previous studies have revealed a lagged connection of the NAO with preceding MJO events (Cassou, 2008; Jiang et al., 2017; Lin et al., 2009). The positive (negative) NAO tends to follow the enhanced (reduced) convection over the Indian Ocean at a lag of 10–15 days, which corresponds to the MJO phase 3 (phase 6). Such a lagged connection is reproduced well both in simplified general circulation models (GCMs) forced with the fixed MJO heating (Lin & Brunet, 2018; Shao et al., 2019) and in fully coupled atmosphere-ocean models forced with the eastward-moving MJO heating (Straus et al., 2015; Yadav et al., 2019). This suggests that the MJO's leading impact on the NAO is a robust intrinsic feature of the atmosphere. Thus it provides an important source for subseasonal predictability of the NAO (Lin et al., 2010; Tseng et al., 2018).

Physically, the MJO's impact on the NAO may originate from the MJO-excited Rossby wave propagation toward the North Atlantic and its subsequent interaction with synoptic eddies locally (Cassou, 2008; Lin et al., 2009). An initiation of Rossby wave trains in the Pacific and the interactions among the transient eddies from the eastern Pacific during the MJO phase 3 (phase 6) are considered to be responsible for setting the positive (negative) NAO phase (Rivière & Drouard, 2015; Fromang & Rivière, 2020). Another pathway of influence was suggested by Lin et al. (2015), who indicated that the MJO convection anomaly over the Indian Ocean may induce a disturbance in the South Asian jet that propagates along the midlatitude waveguide (e.g., Branstator, 2002) and affects the NAO. In addition to the wave train across the North Pacific, Shao et al. (2019) found that the MJO heating initiates an upstream and westward propagation of disturbances to western Asia-Europe along the Asian subtropical jet. Lin and Brunet (2018) also revealed an early influence of a westward propagating Rossby wave excited by the MJO. This suggests the possibility of multiple pathways for the mechanism of the MJO's influence on the NAO.

To further explore the possible pathways and understand the mechanism for the MJO–NAO connection, it is helpful to isolate the individual contribution of the MJO-related regional and moving heating over the Indian Ocean and the western Pacific. On one hand, the positive heating anomaly over the western Pacific tends to induce a negative-phased NAO (Li et al., 2006b; Lin et al., 2005; Yadav and Straus, 2017), and this influence is sensitively dependent on the longitudinal position of the heating. On the other hand, the tropical Indian Ocean heating induces an NAO tendency toward its positive phase (Hoerling et al., 2004; Li et al., 2006a; Lin et al., 2015; Yu & Lin, 2016). Note that there is potential interference between the effects of the MJO’s Indian Ocean and western Pacific heating, because one excited Rossby wave can alter the background flow and affect the route of a Rossby wave excited by its counterpart.

In order to isolate the individual and combined roles of the MJO-linked regional heating, we use a coupled ocean–atmosphere–land model, CFSv2, to conduct sensitivity experiments. Since the initial state is still important for the extended-range weather forecasting, we use observed initial conditions, but add idealized, temporally evolving heating, designed to mimic realistic propagating MJO heating, to the full coupled model. Such a scheme preserves the information embedded in the initial state containing the preceding MJO’s signal, and thus has advantages over that with fixed heating forcing (Fromang & Rivière, 2020).

## **2 Model and Methods**

### **2.1 Model Experiments**

The coupled model, Climate Forecast System model version 2 (CFSv2) of the National Centers for Environmental Prediction (NCEP), is used. Its atmospheric component model (the Global Forecast System) has a T126 horizontal resolution with 64 vertical levels. The outputs are interpolated to  $1^\circ \times 1^\circ$  resolution and 11 pressure levels. The oceanic component is the Modular Ocean Model version 4 (MOM4) from the Geophysical Fluid Dynamics Laboratory (GFDL). The details of the CFSv2 are described in Saha et al. (2014).

The Control runs consist of four-month reforecasts (1 December to 31 March) beginning from three sets of perturbed initial conditions (ICs) on 1 December of each year over the 31-yr period (1980–2010), thus yielding a total of 93 simulations of 121 days. The ICs for atmosphere, ocean, sea-ice, and land surface are obtained from the CFS Reanalysis (CFSR) (Saha et al.,

2010), of which the atmosphere ICs are perturbed by blending different atmospheric states through a weighted average (e.g., Yadav et al., 2019).

An idealized MJO evolving heating is added to model generated temperature tendency to mimic realistic MJO cycles. Here the idealized MJO heating is prescribed with the spatial pattern and propagating features by combining the technique developed by Jang and Straus (2012) and Straus et al. (2015), and with the vertical profile based on estimates of the total diabatic heating from the tropical rainfall measuring mission (TRMM) as Straus et al. (2015). The technique was also recently applied for model heating bias correction by Swenson et al. (2019). The magnitude and temporal structure of the idealized heating are overall based on observations of Yadav and Straus (2017). Such an added heating, even with a relatively small magnitude, can effectively organize the evolution of tropical diabatic heating in the model to give a robust MJO (Straus et al., 2015).

To understand the model response to isolated MJO cycles, three sets of MJO-heating experiments with heating forcing over different regions are conducted, including the Indo–western Pacific Ocean (MJO\_IP) runs, Indian Ocean (MJO\_IO) runs, and western Pacific (MJO\_WP) runs. All these experiments are listed in Table S1 in the supporting information. Note that the MJO\_IP runs represent the typical MJO cycles, similar to the Slow Repeated Cycles runs in Yadav et al. (2019), except for a smaller ensemble size. A maximum added heating rate of  $0.8 \text{ K d}^{-1}$  was chosen with the overall magnitude scaled, so that the *total* (model generated plus added) heating was roughly close to the observations. A fixed phase speed of  $3^\circ$  longitudes per day was adapted to match the slow cases, yielding a period of 60 days.

Figures 1a–1f display the spatial structure and temporal evolution of the idealized heating for these experiments. The vertical structure of the heating (Figures 1a–1c) indicates an evolution from shallow to deep gradually (Yadav et al., 2019), accompanied by an eastward propagation with two complete MJO cycles (Figures 1d–1f). The added heating decays off the equator as a Gaussian form with an e-folding scale of  $15^\circ$  latitudes (Figure S1). The vertically averaged *total* diabatic heating anomalies are shown in Figures 1g–1i. The diabatic heating in the MJO\_IP runs matches the observational slow MJO cases of Yadav and Straus (2017), except for an amplification by a factor of two. The heating in the MJO\_WP runs is additionally induced over the eastern Indian Ocean centering around  $90^\circ\text{E}$ , lagging that in MJO\_IO runs by about 10 days. This may be caused by the feedback of the mid-latitude waves to tropical convective heating

(Frederiksen & Lin, 2013; Moore et al., 2010). Overall, the prescribed heating mirrors the horizontal structure of the MJO diabatic heating reasonably well (Figure S2).

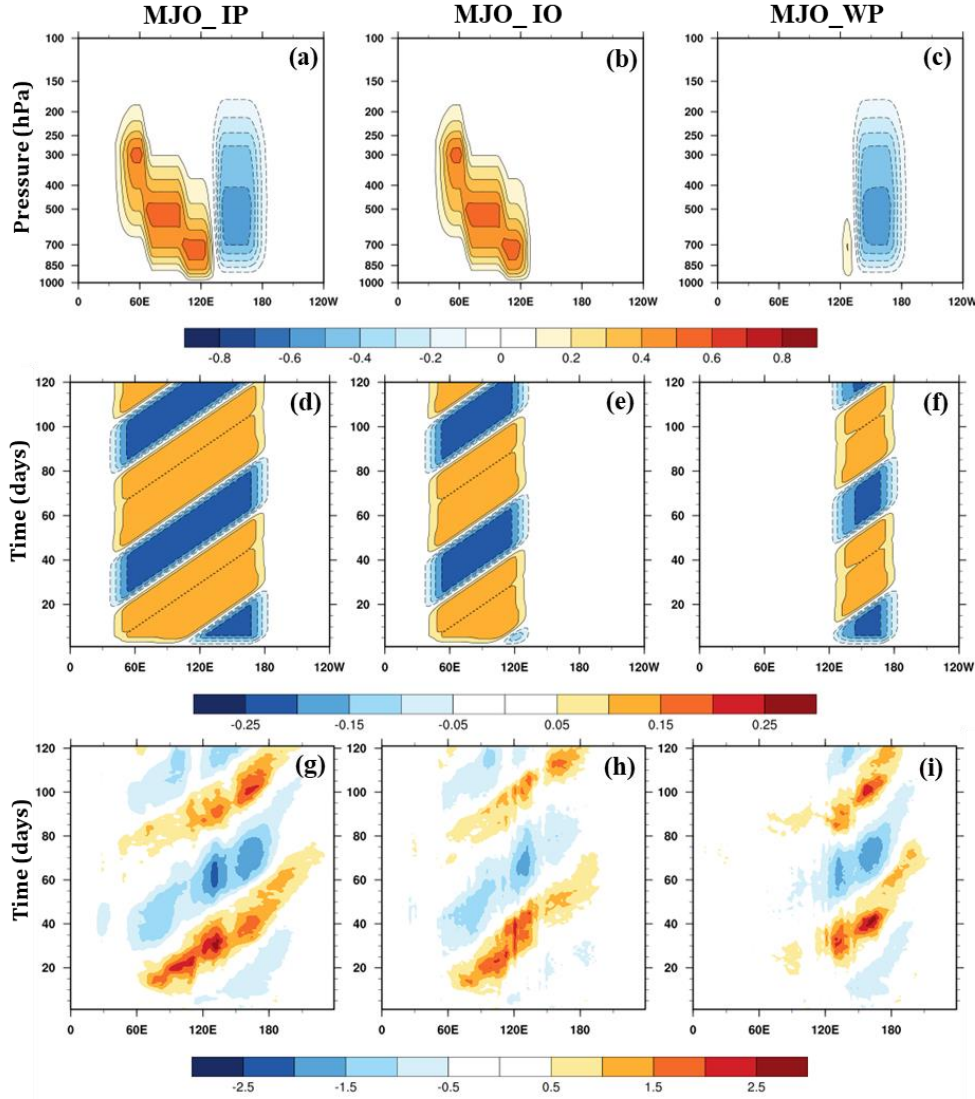


**Figure 1.** The pressure-longitude cross-section of added heating anomalies on day 12 (a–c), vertically averaged (over 1000–50 hPa) added heating anomalies (d–f) and total diabatic heating anomalies (g–i) at each reforecast day. Displayed is the value averaged over latitudes 15°S–15°N. From left to right, it corresponds to MJO\_IP, MJO\_IO, and MJO\_WP runs, respectively. Units are K day<sup>-1</sup>.

## 2.2 Analysis Methods

The NAO pattern is defined as the first empirical orthogonal function (EOF) mode of the daily 500-hPa geopotential height fields (Z500) over the North Atlantic region (20°N–85°N,

90°W–30°E). The daily NAO indices are calculated as the projection of the daily Z500 anomalies onto the NAO pattern; this time series of projections is subsequently normalized. The occurrence probabilities of the positive (negative) phase of the NAO at each reforecast day are obtained by counting the number of days with the daily NAO index greater (less) than 0.5 (-0.5) and then dividing by the total ensemble size of 93. When comparing the contribution of the MJO heating imposed over different regions, the identical NAO pattern in Control runs is used for calculating the NAO index. For each experiment, anomalies are defined as departures from the annual cycle in the Control runs. This model annual cycle is estimated by projecting the daily time series of each winter separately onto the first three Legendre polynomials in time as described in Straus et al. (2003), and then averaging over all winters. We use Fourier decomposition as a spatial filter method to isolate the synoptic-scale (zonal waves 5–12) eddies.

### 3 Results

The NAO pattern in Control runs (Figure 2a) agrees well with that in the ERA-Interim reanalysis (Dee et al., 2011) as shown in Yadav et al. (2019). For the MJO\_IP runs, the NAO pattern is similar to that in Control runs, with a slightly stronger amplitude over the positive sector (Figure 2b). As the model simulates both the evolving MJO cycles and the NAO pattern well, we first investigate whether the observed MJO–NAO linkage can be reproduced in the MJO\_IP runs. Figure S3 illustrates the occurrence probabilities of the NAO at each reforecast day in the MJO\_IP runs. For the first (second) cycle, the occurrence probabilities of the positive NAO are increased about 10–15 days after the MJO heating reaches roughly the 90°E longitude at around day 15 (80). Conversely, the increase of the negative NAO occurs 15–20 days following the MJO heating (cooling) over the western Pacific (Indian Ocean) at around day 40. This suggests that the MJO–NAO connection can be captured well by forcing this coupled model with the anomalous heating associated with the MJO cycles.

In order to compare the contribution of the MJO heating over different regions, the evolution of NAO index from day 1 to 121 in each experiment is displayed (Figure 2c). Similar to the occurrence probabilities, the averaged NAO indices show fluctuations of roughly two cycles. During the first 10 days, the NAO indices in each MJO-heating runs are close to that in Control runs. After day 15, the NAO index in MJO\_IO runs begins to increase until around day 30. Generally, the increase of the NAO index in MJO\_IO runs leads that in MJO\_WP runs for

about 10 days during the first cycle. This indicates that the positive NAO anomaly may be firstly initiated by the Indian Ocean heating of the MJO. Note that the NAO indices in the second cycles display relatively weaker amplitudes to those in the first cycles, in coincidence with the somewhat weaker MJO heating anomalies over the Indian Ocean. As complex tropical-extratropical interactions are involved in the second cycle, we mainly focus on the NAO-like response in the first cycle.

It is difficult to directly interpret the NAO-like response to the MJO-related regional forcing because the additional heating over the Indian Ocean (western Pacific) are induced in the MJO\_WP (MJO\_IO) runs. To isolate the contribution of the MJO forcing over the western Pacific, we examine the differences in the heating (see Figure S4a) and response between the MJO\_IP and MJO\_IO runs. The differences of Z500 over the North Atlantic between the MJO\_IP and MJO\_IO runs, and between the MJO\_IP (MJO\_IO) and Control runs, are projected onto the NAO pattern in Control runs. Figure 2d displays the projection indices of the Z500 differences for the MJO\_IP minus MJO\_IO runs (green curve), MJO\_IP minus Control runs (red curve), and MJO\_IO minus Control runs (blue curve). The green curve shows that the MJO heating over the western Pacific only contributes at a later stage. In contrast, the blue curve indicates a dominant role of the anomalous Indian Ocean heating on the NAO anomaly. The 200-hpa streamfunction together with wave activity vectors for the raw MJO\_IP runs demonstrate that the MJO-initiated Rossby waves originate mostly from the Indian Ocean heating/cooling region (Figure S5). Seo and Son (2012) showed that the Indian Ocean heating can generate a much broader and stronger Rossby wave source because of its position relative to the subtropical jet, where the relative vorticity is large. This further verifies the crucial role the anomalous MJO heating over the Indian Ocean. Thus, we will concentrate on the response to the heating forcing in the MJO\_IO runs.



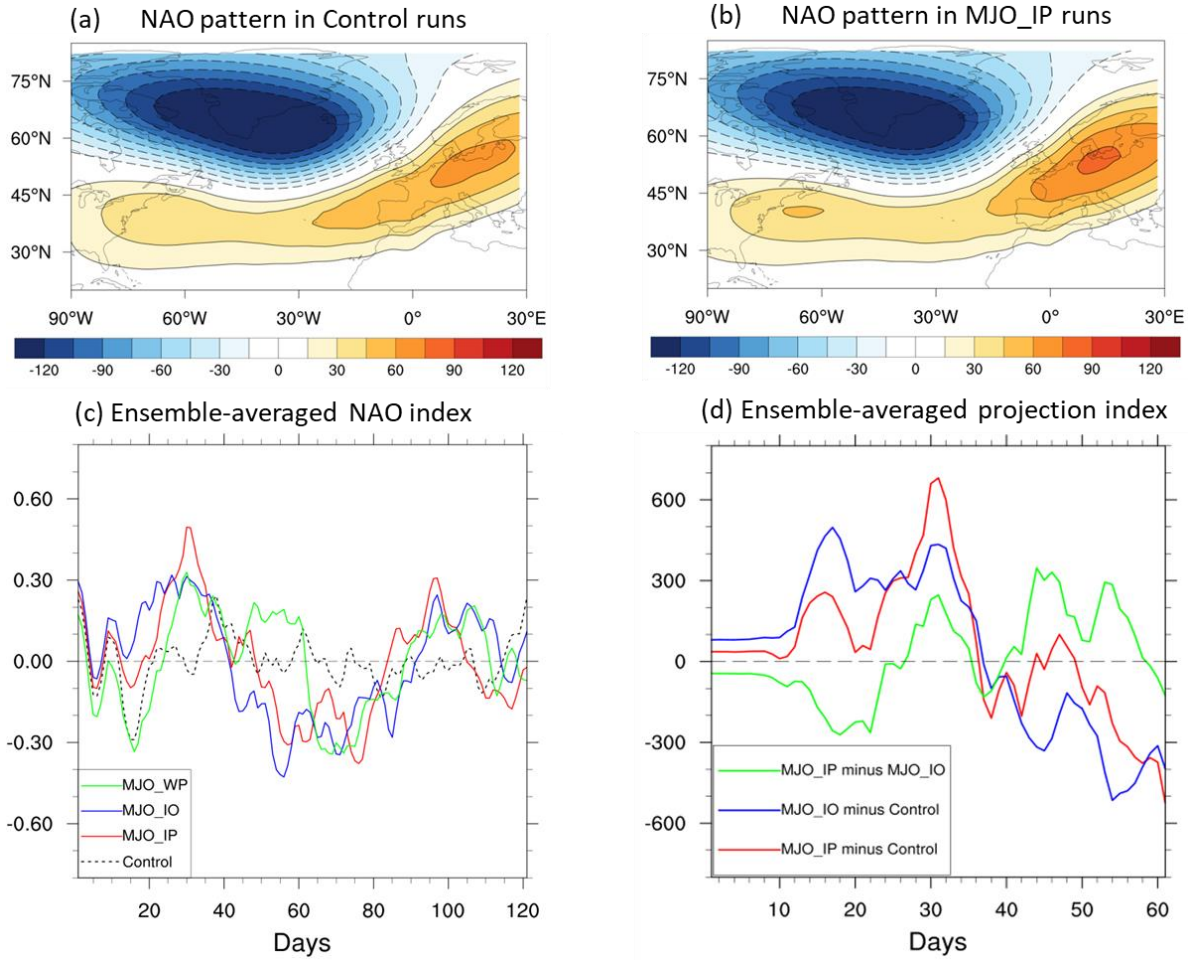


**Figure 2.** The 500-hpa geopotential height (Z500) anomalies (unit: gpm) regressed onto the NAO index in (a) Control runs and (b) MJO\_IP runs, together with (c) ensemble-averaged NAO index at each reforecast day for the MJO\_IP (red curve), MJO\_IO (blue curve), MJO\_WP (green curve) and Control runs (black curve), and (d) projection indices of the Z500 differences for the MJO\_IP minus MJO\_IO runs (green curve), the MJO\_IP minus Control runs (red curve), and the MJO\_IO minus Control runs (blue curve), respectively.

The differences of the Z500 between the MJO\_IO and Control runs from day 7 to day 21 are shown in Figure 3, which illustrates the evolution of the extratropical response to the MJO heating. Since the diabatic heating anomaly over the Indian Ocean does not appear until around day 7 (see Figure S4b), there is no evident response before day 11. From day 13 to day 15, negative anomalies of the geopotential height are built up over the subtropical Asia and extend northwestward. There is also formation of an anomalous anticyclone over the western North

Pacific, along with a north–south dipole over the eastern North Pacific. Over the high latitudes of the North Atlantic, a negative height anomaly is formed, which deepens over the Greenland region until day 17. Meanwhile, a positive height anomaly to the northwest of the Indian Ocean extends westward, merging with the one over the subtropical North Atlantic, together forming the southern part of the NAO-like pattern. Thus, a positive NAO-like pattern is developed. Delayed by 15–20 days from the cooling over the Indian Ocean (see Figure S4b), a strong negative NAO-like response is developed at around days 55–61 (Figure S6). Prior to the formation of negative NAO anomaly, the positive height anomalies over the Eurasia and negative height anomalies over the North Pacific are established respectively, which are generally reversed to the situation following the heating over the Indian Ocean.

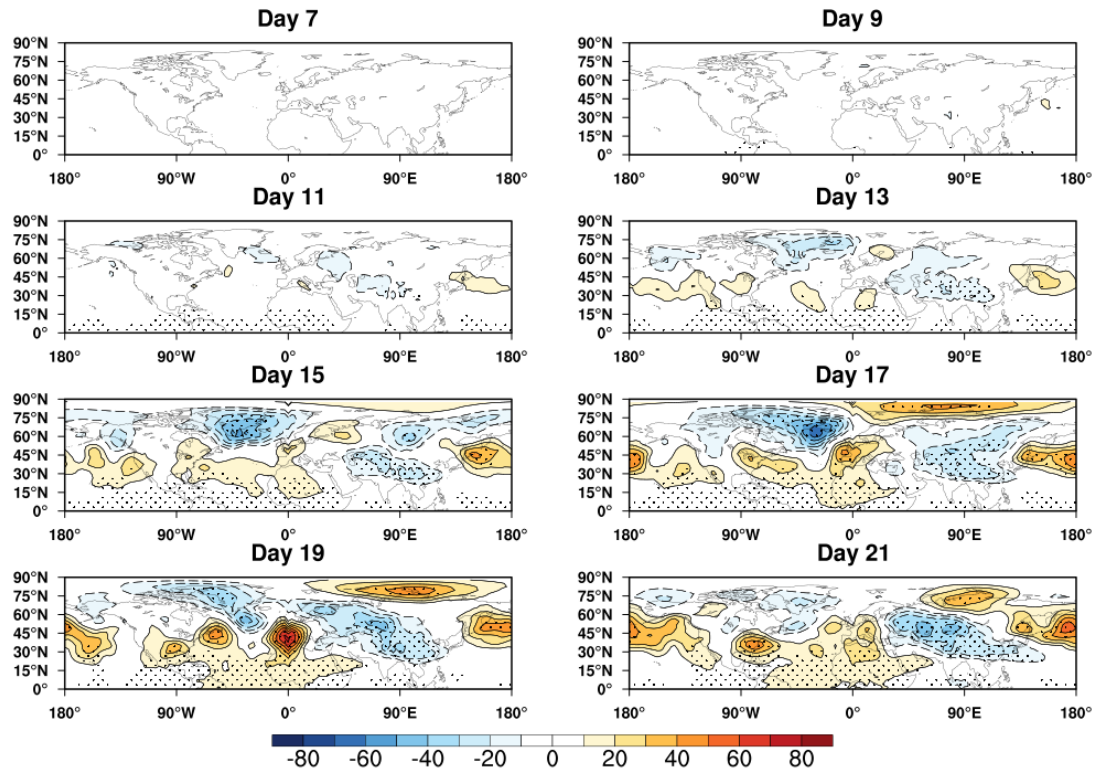


**Figure 3.** Composite differences of the 500-hPa geopotential height (unit: gpm) between the MJO\_IO and Control runs from day 7 to day 21. Dotted is significant at the 90% confidence level according to a Student's *t* test.

Because the subtropical jet can act as a waveguide to modulate the wave/eddy propagation (Lee et al., 2019; Zheng & Chang, 2020), we further investigate the differences of the zonal wind at 300 hpa between the MJO\_IO and Control runs (Figure S7). At the initial stage (days 7–12), a

positive zonal wind anomaly is induced over the subtropical Asian region and enhances with both westward and eastward extension. At days 13–15, a positive zonal wind anomaly is formed over the mid-latitudes of North Atlantic. Then it strengthens and exhibits a poleward shift at days 16–18, along with a negative anomaly built up to its south. This suggests that the North Atlantic mid-latitude jet is pushing northward, in favor of the formation of the positive NAO anomaly.

To understand how the anomalous subtropical Asian jet related to the MJO modulates the North Atlantic jet, we examine the shift in the storm tracks. Figure S8 shows the evolution of the 300-hPa synoptic-scale  $v'v'$  anomaly (the difference between the MJO\_IO and Control runs). At days 10–12, the positive  $v'v'$  anomalies are established along the South Asia jet, which extend to the western Europe at days 13–15, indicating an expanding of Asian storm track influencing the western Europe directly. Subsequently, the storm tracks are enhanced over the eastern North Atlantic. In addition, the strengthening storm tracks over the North Pacific exhibit an eastward extension, which seem to influence the North Atlantic at days 22–24. Both eastward and westward extension of the enhanced storm tracks are likely to contribute to the positive NAO anomaly. On the contrary, the weakened subtropical Asian jet (at days 43–45) and the subsequent weakening storm tracks (at around days 49–57) over the North Atlantic are conducive to the negative NAO anomaly.

In order to detect the pathways via which the MJO-induced disturbances propagate into the North Atlantic, we further calculate the one-point lead-lag correlation of the 300-hPa synoptic-scale meridional wind anomaly ( $v'$ ), where a base point is chosen nearby the subtropical Asian jet at 60°E, 30°N. The lead-lag correlation coefficients are presented as a function of time and longitude, averaged from 30°N to 40°N (Figure 4). Consistent with the westerly jet stream, the synoptic eddies generally exhibit eastward movement. The westward propagation indicated by the dashed line in Figure 4a suggests that the synoptic eddies over the North Atlantic at around days 12–15 may be affected by those from the South Asia jet. From day 16 to 18, the synoptic eddies over the North Atlantic in MJO\_IO runs exhibit a faster eastward phase speed with respect to those in Control runs, along with a northeast–southwest tilt (Figure S9), favoring the development of the positive NAO phase (e.g., Ren et al., 2012; Song, 2016). As such, the anomalies along the Asian subtropical jet may firstly influence the positive NAO through the westward Asian-Europe pathway.

On the other hand, the disturbances induced along the subtropical Asian jet propagate across the North Pacific and downstream into the North Atlantic from day 12 to day 28. The increase of the projection index later at around days 22–30 (see Figure 2d) could be largely attributed to the Pacific pathway. This also suggests that it takes a longer time for the MJO heating over the Indian Ocean to affect the NAO via the Pacific pathway than the westward pathway. The eastward tilt of the lines in Figure 4b shows a more traditional Pacific pathway (at days 45–60) for the negative NAO-like responses at around days 55–60, while the westward pathway is much weaker. This indicates that the Eurasian pathway may play a secondary role.

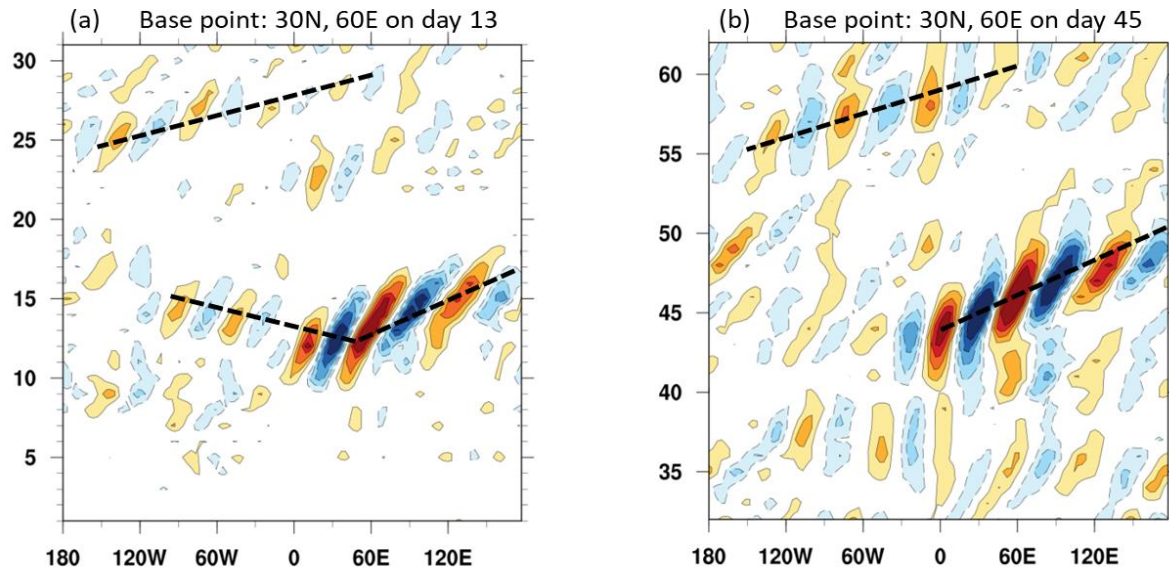


**Figure 4.** One-point lead-lag correlation coefficients of 300-hpa synoptic-scale  $v'$  for a base point at 30°N, 60°E on day 13 (a) and day 45 (b), averaged over the latitudes 30°N–40°N. Here,  $v'$  is the difference of the meridional wind (waves 5–12) between the MJO\_IO and Control runs. The ordinate is reforecast time. The interval of the contours is 0.1.

#### 4 Summary and Discussions

The mechanism for the observed lagged-connection of the NAO with the MJO is investigated by forcing a coupled model (CFSv2) with idealized cyclic MJO heatings. Three sets of experiments, each having an integration of two eastward propagating MJO cycles with a period of about 60 days, are conducted to isolate the contribution of the MJO-related heating anomalies over the Indian Ocean and western Pacific, respectively. The results demonstrate an increase of the positive (negative) NAO occurrence following the MJO heating (cooling) over the Indian Ocean at a lag of 10–15 (15–20) days. Furthermore, the anomalous MJO heating over

the Indian Ocean, rather than that over the western Pacific, dominates the NAO-like response. The MJO heating over the Indian Ocean can exert its influence via the traditional pathway across the North Pacific, however part of the impact may be transmitted via the Eurasia, which takes a shorter time (around 7–10 days). The shift of the strengthened subtropical Asian jet causes an expanding Asian storm track to propagate westward, influencing the Europe and enhancing the storm tracks over the eastern North Atlantic, thus favoring the development of the positive NAO. On the other hand, the induced disturbances in the subtropical Asian jet propagate across the North Pacific and downstream into the North Atlantic, enhancing the NAO after around 10–15 days. The situation is essentially reversed following the MJO's cooling over the Indian Ocean for the negative NAO-like response, although the Eurasian pathway does not seem to play a role here.

Since the MJO-related heating anomalies over the Indian Ocean and the western Pacific are not independent, and presumably feed back on each other, the dominant effect of the anomalous MJO heating over the Indian Ocean does not rule out the potential role of the heating over the western Pacific. The western Pacific heating anomaly has minor contribution, probably because the affected initial state of the portion of the subtropical jet is less effective in transporting the disturbances along the jet waveguide to the North Atlantic (e.g., Lin & Brunet, 2018).

While we have shed light on the direct MJO-related tropical forcing of the North Atlantic region, other mechanisms are likely to play a role, such as the possible stratosphere pathway (e.g., Barnes et al., 2019; Lee et al., 2019). There are also tropical–extratropical interactions of intraseasonal oscillations (Frederiksen & Lin, 2013), which may play a role in the model experiments. For example, the synoptic eddies from the North Atlantic jet may affect those along the subtropical jet, which in turn have an influence on the North Atlantic jet through downstream propagation. The mechanism for how the extratropics influence the tropical heating linked to the MJO deserves further investigation.

## **Acknowledgments**

This study was jointly supported by the National Key Research and Development Program of China (2018YFA0606403), the Fundamental Research Funds for the Central Universities (2018B06714), and the National Natural Science Foundation of China (41790473 and

41421004). We thank Drs. Chul-Su Shin and Bohua Huang for assisting in the model experiments. This work used the Extreme Science and Engineering Discovery Environment (XSEDE) computing resource Stampede, which is supported by the National Science Foundation (grant number ACI-1548562). The ERA-Interim reanalysis data are available on the European Centre for Medium-Range Weather Forecasts (ECMWF) website (<https://apps.ecmwf.int/datasets/data/interim-full-daily/levtype=pl/>). The NCEP Climate Forecast System Reanalysis (CFSR) can be obtained from <https://climatedataguide.ucar.edu/climate-data/climate-forecast-system-reanalysis-cfsr>.

## References

- Barnes, E. A., Samarasinghe, S., Ebertuphoff, I., & Furtado, J. C. (2019). Tropospheric and stratospheric causal pathways between the MJO and NAO. *Journal of Geophysical Research*, 124(16), 9356–9371. <https://doi.org/10.1029/2019JD031024>
- Branstator, G. (2002). Circumglobal teleconnections, the jet stream waveguide, and the North Atlantic Oscillation. *Journal of Climate*, 15(14), 1893–1910. [https://doi.org/10.1175/1520-0442\(2002\)015<1893:CTTJSW>2.0.CO;2](https://doi.org/10.1175/1520-0442(2002)015<1893:CTTJSW>2.0.CO;2)
- Cassou, C. (2008). Intraseasonal interaction between the Madden-Julian Oscillation and the North Atlantic Oscillation. *Nature*, 455(7212), 523–527. <https://doi.org/10.1038/nature07286>
- Dee, D. P., Uppala, S. M., Simmons, A. J., Berrisford, P., Poli, P., Kobayashi, S., et al. (2011). The ERA-Interim reanalysis: Configuration and performance of the data assimilation system. *Quarterly Journal of the Royal Meteorological Society*, 137(656), 553–597. <https://doi.org/10.1002/qj.828>
- Frederiksen, J. S., & Lin, H. (2013). Tropical–extratropical interactions of intraseasonal oscillations. *Journal of the Atmospheric Sciences*, 70(10), 3180–3197. <https://doi.org/10.1175/JAS-D-12-0302.1>
- Fromang, S., & Rivière, G. (2020). The effect of the Madden–Julian Oscillation on the North Atlantic Oscillation using idealized numerical experiments. *Journal of the Atmospheric Sciences*, 77(5), 1613–1635. <https://doi.org/10.1175/JAS-D-19-0178.1>
- Garfinkel, C. I., Benedict, J. J., & Maloney, E. D. (2014). Impact of the MJO on the boreal winter extratropical circulation. *Geophysical Research Letters*, 41(16), 6055–6062. <https://doi.org/10.1002/2014GL061094>
- Hoerling, M. P., Hurrell, J. W., Xu, T., Bates, G. T., & Phillips, A. S. (2004). Twentieth century North Atlantic climate change. Part ii: Understanding the effect of Indian Ocean warming. *Climate Dynamics*, 23(3), 391–405. <https://doi.org/10.1007/s00382-004-0433-x>

- Hurrell, J. W., Kushnir, Y., Ottersen, G., & Visbeck, M. (2003). An overview of the North Atlantic Oscillation. In J. W. Hurrell, Y. Kushnir, G. Ottersen, & M. Visbeck (Eds.), *The North Atlantic Oscillation: Climatic Significance and Environmental Impact, Geophysical Monograph Series* (Vol. 134, pp. 1–35). Washington, DC: American Geophysical Union.
- Jang, Y., & Straus, D. M. (2012). The Indian monsoon circulation response to El Niño diabatic heating. *Journal of Climate*, 25(21), 7487–7508. <https://doi.org/10.1175/JCLI-D-11-00637.1>
- Jiang, Z., Feldstein, S. B., & Lee, S. (2017). The relationship between the Madden-Julian Oscillation and the North Atlantic Oscillation. *Quarterly Journal of the Royal Meteorological Society*, 143(702), 240–250. <https://doi.org/10.1002/qj.2917>
- Lee, R. W., Woolnough, S. J., Charlton-Perez, A. J., & Vitart, F. (2019). ENSO modulation of MJO teleconnections to the North Atlantic and Europe. *Geophysical Research Letters*, 46(22), 13535–13545. <https://doi.org/10.1029/2019GL084683>
- Li, S., Hoerling, M. P., & Peng, S. (2006a). Coupled ocean-atmosphere response to Indian Ocean warmth. *Geophysical Research Letters*, 33(7), L07713. <https://doi.org/10.1029/2005GL025558>
- Li, S., Hoerling, M. P., Peng, S., & Weickmann, K. M. (2006b). The annular response to tropical pacific SST forcing. *Journal of Climate*, 19(9), 1802–1819. <https://doi.org/10.1175/JCLI3668.1>
- Lin, H., & Brunet, G. (2018). Extratropical response to the MJO: Nonlinearity and sensitivity to the initial state. *Journal of the Atmospheric Sciences*, 75(1), 219–234. <https://doi.org/10.1175/JAS-D-17-0189.1>
- Lin, H., Brunet, G., & Derome, J. (2009). An observed connection between the North Atlantic Oscillation and the Madden-Julian Oscillation. *Journal of Climate*, 22(2), 364–380. <https://doi.org/10.1175/2008JCLI2515.1>
- Lin, H., Brunet, G., & Fontecilla, J. S. (2010). Impact of the Madden-Julian Oscillation on the intraseasonal forecast skill of the North Atlantic Oscillation. *Geophysical Research Letters*, 37(19), L19803. <https://doi.org/10.1029/2010GL044315>
- Lin, H., Brunet, G., & Yu, B. (2015). Interannual variability of the Madden-Julian Oscillation and its impact on the North Atlantic Oscillation in the boreal winter. *Geophysical Research Letters*, 42(13), 5571–5576. <https://doi.org/10.1002/2015GL064547>
- Lin, H., Derome, J., & Brunet, G. (2005). Tropical Pacific link to the two dominant patterns of atmospheric variability. *Geophysical Research Letters*, 32(3), L03801. <https://doi.org/10.1029/2004GL021495>
- Luo, D., Lupo, A. R., & Wan, H. (2007). Dynamics of eddy-driven low-frequency dipole modes. Part i: A simple model of North Atlantic Oscillations. *Journal of the Atmospheric Sciences*, 64(1), 3–28. <https://doi.org/10.1175/JAS3818.1>



- 381 Luo, D., Zhong, L., & Franzke, C. L. E. (2015). Inverse energy cascades in an eddy-induced NAO-type flow:  
382 Scale interaction mechanism. *Journal of the Atmospheric Sciences*, 72(9), 3417–3448.  
383 <https://doi.org/10.1175/JAS-D-15-0062.1>
- 384 Madden, R. A., & Julian, P. R. (1994). Observations of the 40–50-day tropical oscillation—a review. *Monthly*  
385 *Weather Review*, 122(5), 814–837. [https://doi.org/10.1175/1520-](https://doi.org/10.1175/1520-0493(1994)122<0814:OOTDIO>2.0.CO;2)  
386 [0493\(1994\)122<0814:OOTDIO>2.0.CO;2](https://doi.org/10.1175/1520-0493(1994)122<0814:OOTDIO>2.0.CO;2)
- 387 Matthews, A. J., Hoskins, B. J., & Masutani, M. (2004). The global response to tropical heating in the  
388 Madden–Julian Oscillation during the northern winter. *Quarterly Journal of the Royal Meteorological*  
389 *Society*, 130(601), 1991–2011. <https://doi.org/10.1256/qj.02.123>.
- 390 Moore, R. W., Martius, O., & Spengler, T. (2010). The modulation of the subtropical and extratropical  
391 atmosphere in the Pacific basin in response to the Madden–Julian Oscillation. *Monthly Weather*  
392 *Review*, 138(7), 2761–2779. <https://doi.org/10.1175/2010MWR3194.1>
- 393 Ren, H.-L., Jin, F.-F., & Gao, L. (2012). Anatomy of synoptic eddy–NAO interaction through eddy structure  
394 decomposition. *Journal of the Atmospheric Sciences*, 69(7), 2171–2191. [https://doi.org/10.1175/JAS-](https://doi.org/10.1175/JAS-D-11-069.1)  
395 [D-11-069.1](https://doi.org/10.1175/JAS-D-11-069.1)
- 396 Rivière, G., & Drouard, M. (2015). Dynamics of the Northern Annular Mode at weekly time scales. *Journal of*  
397 *the Atmospheric Sciences*, 72(12), 4569–4590. <https://doi.org/10.1175/JAS-D-15-0069.1>
- 398 Saha, S., Moorthi, S., Pan, H., Wu, X., Wang, J., Nadiga, S., et al. (2010). The NCEP climate forecast system  
399 reanalysis. *Bulletin of the American Meteorological Society*, 91(8), 1015–1057.  
400 <https://doi.org/10.1175/2010BAMS3001.1>
- 401 Saha, S., Moorthi, S., Wu, X., Wang, J., Nadiga, S., Tripp, P., et al. (2014). The NCEP climate forecast system  
402 version 2. *Journal of Climate*, 27(6), 2185–2208. <https://doi.org/10.1175/JCLI-D-12-00823.1>
- 403 Seo, K.-H., & Son, S.-W. (2012). The global atmospheric circulation response to tropical diabatic heating  
404 associated with the Madden–Julian Oscillation during northern winter. *Journal of the Atmospheric*  
405 *Sciences*, 69(1), 79–96. <https://doi.org/10.1175/2011JAS3686.1>
- 406 Shao, X., Song, J., & Li, S. (2019). The lagged connection of the positive NAO with the MJO phase 3 in a  
407 simplified atmospheric model. *Theoretical and Applied Climatology*, 135(3), 1091–1103.  
408 <https://doi.org/10.1007/s00704-018-2425-5>
- 409 Song, J. (2016). Understanding anomalous eddy vorticity forcing in North Atlantic Oscillation events. *Journal*  
410 *of the Atmospheric Sciences*, 73(8), 2985–3007. <https://doi.org/10.1175/JAS-D-15-0253.1>
- 411 Stan, C., Straus, D. M., Frederiksen, J. S., Lin, H., Maloney, E. D., & Schumacher, C. (2017). Review of  
412 tropical–extratropical teleconnections on intraseasonal time scales. *Reviews of Geophysics*, 55(4),  
413 902–937. <https://doi.org/10.1002/2016RG000538>



- Straus, D. M., Shukla, J., Paolino, D. A., Schubert, S. D., Suarez, M. J., Pegion, P., & Kumar, A. (2003). Predictability of the seasonal mean atmospheric circulation during autumn, winter, and spring. *Journal of Climate*, 16(22), 3629–3649. [https://doi.org/10.1175/1520-0442\(2003\)016<3629:POTSMA>2.0.CO;2](https://doi.org/10.1175/1520-0442(2003)016<3629:POTSMA>2.0.CO;2)
- Straus, D. M., Swenson, E. T., & Lappen, C.-L. (2015). The MJO cycle forcing of the North Atlantic circulation: Intervention experiments with the community earth system model. *Journal of the Atmospheric Sciences*, 72(2), 660–681. <https://doi.org/10.1175/JAS-D-14-0145.1>
- Swenson, E. T., Straus, D. M., Snide, C. E., & Fahad, A. A. (2019). The role of tropical heating and internal variability in the California response to the 2015/16 ENSO event. *Journal of the Atmospheric Sciences*, 76(10), 3115–3128. <https://doi.org/10.1175/JAS-D-19-0064.1>
- Tseng, K. C., Barnes, E. A., & Maloney, E. D. (2018). Prediction of the midlatitude response to strong Madden-Julian Oscillation events on S2S time scales. *Geophysical Research Letters*, 45(1), 463–470. <https://doi.org/10.1002/2017GL075734>
- Yadav, P., & Straus, D. M. (2017). Circulation response to fast and slow MJO episodes. *Monthly Weather Review*, 145 (5), 1577–1596. <https://doi.org/10.1175/MWR-D-16-0352.1>
- Yadav, P., Straus, D. M., & Swenson, E. T. (2019). The Euro-Atlantic circulation response to the Madden-Julian Oscillation cycle of tropical heating: Coupled GCM intervention experiments. *Atmosphere-Ocean*, 57(3), 161–181. <https://doi.org/10.1080/07055900.2019.1626214>
- Yu, B., & Lin, H. (2016). Tropical atmospheric forcing of the wintertime North Atlantic Oscillation. *Journal of Climate*, 29(5), 1755–1772. <https://doi.org/10.1175/JCLI-D-15-0583.1>
- Zhang, C. (2005). Madden-Julian Oscillation. *Reviews of Geophysics*, 43(2), RG2003. <https://doi.org/10.1029/2004RG000158>
- Zheng, C., & Chang, E. K. M. (2019). The role of MJO propagation, lifetime, and intensity on modulating the temporal evolution of the MJO extratropical response. *Journal of Geophysical Research: Atmospheres*, 124(10), 5352–5378. <https://doi.org/10.1029/2019JD030258>
- Zheng, C., & Chang, E. K. M. (2020). The role of extratropical background flow in modulating the MJO extratropical response. *Journal of Climate*, 33(11), 4513–4536. <https://doi.org/10.1175/JCLI-D-19-0708.1>

## References From the Supporting Information

- Takaya, K., & Nakamura H. (2001). A formulation of a phase-independent wave-activity flux for stationary and migratory quasigeostrophic eddies on a zonally varying basic flow. *Journal of the Atmospheric Sciences*, 58(6), 608–627. [https://doi.org/10.1175/1520-0469\(2001\)058<0608:AFOAPI>2.0.CO;2](https://doi.org/10.1175/1520-0469(2001)058<0608:AFOAPI>2.0.CO;2)